

Optical polarization and near IR photometry of the proto-planetary nebula Hen 3-1475¹

Cláudia V. Rodrigues², Francisco J. Jablonski², Jane Gregorio-Hetem³, Gabriel R. Hicckel^{2,4}
and Marília J. Sartori^{5,3}
claudia@das.inpe.br

ABSTRACT

We present BVRI CCD aperture polarization and near-infrared photometry of the proto-planetary nebula Hen 3-1475. Its intrinsic polarization is high and shows a strong spectral dependence. The position angles in all bands are perpendicular to the axis of the observed bipolar structure. A Monte Carlo code is used to model the intrinsic polarization of Hen 3-1475. Using disk dimensions and other constraints suggested by previous works, we are able to reproduce the observations with an optically thick disk composed by grains with a power-law size distribution ranging from 0.06 to 0.22 μm . We also reliably estimate the foreground polarization from hundreds of stars contained in the CCD images. It is parallel to the intrinsic polarization of Hen 3-1475. Possible implications of this result are discussed. From IR observations, we estimate a interstellar reddening, A_V , of about 3.2.

Subject headings: stars: individual (Hen 3-1475)—planetary nebulae: individual (Hen 3-1475)—circumstellar matter—polarization—radiative transfer

1. Introduction

Hen 3-1475 (IRAS 17423-1755) is identified as a proto-planetary nebula (PPN), i.e., an object between the end of the asymptotic giant branch (AGB) and the planetary nebula (PN) phases. The classification and physical properties of Hen 3-1475 are supported by a broad base of observational data: radio emission (Knapp et al. 1995); OH masers (te Lintel Hekkert 1991; Zijlstra et al. 2001); optical imaging and spectroscopy (Riera

et al. 1995; Bobrowski et al. 1995; Borkowski, Blondin, & Harrington 1997; Borkowski & Harrington 2001). Probably the strongest evidence in favor of its evolutionary stage is the high N abundance, typical of evolved objects, specifically of Type I PN (Riera et al. 1995). The radio continuum indicates the presence of a compact ionized region surrounding the central B star with an estimated dynamical age of only 15 years (Knapp et al. 1995). Recently, Borkowski & Harrington (2001) have obtained images and detailed spectroscopic observations and, among other results, they have derived a distance of 8 kpc, which implies a very high luminosity ($25\,000 L_{\odot}$) for a AGB star at the Galactic Bulge. Analyzing $H\alpha$ spectra, Sánchez Contreras & Sahai (2001) could identify two winds, one of which is probably associated with the post-AGB wind before its interaction with the previous AGB wind.

High-resolution optical images of Hen 3-1475 show a very complex bipolar morphology (Borkowski et al. 1997; Bobrowski et al. 1995; Riera et al. 1995). The central region is dense, probably a

²Instituto Nacional de Pesquisas Espaciais/MCT — Av. dos Astronautas, 1758 — 12227-010 - São José dos Campos - SP — Brazil

³Instituto de Astronomia, Geofísica e Ciências Atmosféricas/USP — Rua do Matão, 1226 — 05508-900 - São Paulo - SP — Brazil

⁴Universidade do Vale do Paraíba - IP&D — Av. Shishima Hifumi, 2911 — 12244-000 - São José dos Campos - SP — Brazil

⁵Laboratório Nacional de Astrofísica/MCT — Rua Estados Unidos, 154 — 37504-364 - Itajubá - MG — Brazil

¹Based on observations made at Laboratório Nacional de Astrofísica/MCT, Brazil

dust disk, which may be responsible for the OH maser emission as well as for the CaII and FeII lines observed in its near-infrared spectrum. This structure has an angular size of about $2''$. The high resolution image obtained by Borkowski et al. (1997) shows also dark patches probably associated with denser clumps of material in the disk. A complex structure of highly collimated optical jets with pairs of point-symmetrical shock-excited knots produces a characteristic S-shaped sequence, which is about $15''$ in size oriented along PA 135° .

In the rapid evolutionary phase of PPN, dramatic changes in geometrical and physical properties of its central star and circumstellar material take place. An example is the development of non-symmetric geometries (eg., bipolar nebulae) in post-AGB objects. The interaction between an equatorial enhanced AGB wind and that from an early PN phase was suggested as a mechanism to produce the variety of geometries seen in PPNe and PNe (Kahn & West 1985). The status of this and other models is reviewed by Frank (2000). This enhanced equatorial wind - which we will call disk - can also play a role in collimating the jets seen in many objects. Recently, Frank, Lery, & Blackman (2002) have shown that a magnetic-centrifugal launching model can explain winds with velocities as high as those observed in Hen 3-1475. Therefore, a good representation of the disk properties is crucial to understand the changes occurring during the PPN phase.

Polarimetry is an useful tool in the study of PNe and PPNe because it is sensitive to the circumstellar geometry and composition. The polarization measured in PPNe is usually high due to the scattering in asymmetric circumstellar environments. Johnson & Jones (1991) have shown that, from red giants to PNe, the evolutionary stage of PPN is the one in which the polarization tends to be highest and that the transition from a spherically symmetric envelope (typical of red giants) to a non-spherical envelope seems to occur in early stages of the AGB phase. The wavelength dependence of the polarization in PPNe has various shapes and some objects present polarization-angle rotation (Trammell, Dinerstein, & Goodrich 1994). Many extended objects were observed using imaging polarimetry (e.g., Scarrot & Scarrot 1995; Gledhill et al. 2001). Far from the central

source, the light is highly polarized and exhibits the centro-symmetric pattern typical of reflection nebulae. However, the polarization near the central object tends to be parallel to the optically thick disk originated in the AGB phase. This pattern is also observed in young stellar objects with bipolar geometries (see references in Bastien & Menard 1988 - Table 1).

In spite of the importance of grain size in the study of the temperature profile and, consequently, of the infrared (IR) luminosity (Stasińska & Szczerba 1999, 2001), few works have focused on the determination of the grain size distribution in PPNe and PNe. An example of model that considers the grain sizes as free parameters is found in Meixner et al. (2002). That work, however, modeled the observed spectral energy distribution (SED) alone. Recent results (Carciofi, Bjorkman, & Magalhães 2002; Li & Lunine 2002) show that the SED alone does not constrain the grain sizes. The spectral dependence of the polarization helps to restrict the models to the dust size distribution (Carciofi, Magalhães, & Bjorkman 2002). Heckert & Smith (1988) modeled the polarization of OH 0739-14 considering single scattering in an envelope composed by grains of a single size. Johnson & Jones (1991) have modeled the observed polarization of some PPNe, but they used a fixed MRN size distribution ranging from 0.005 to $0.10 \mu\text{m}$. To our knowledge, there is no previous attempt to describe the polarization data of a PPN with a free distribution of grain sizes and multiple scattering.

In this work, we present data on broad band CCD aperture polarimetry as well as near-infrared (NIR) photometry of Hen 3-1475 (Section 2). In Section 3 the NIR photometry is analyzed in order to provide information on the interstellar (IS) and intrinsic reddening. The polarimetric observations are discussed and modeled in Section 4 providing some information about the Hen 3-1475 dusty envelope. In the last section, the main conclusions are listed.

2. Observations

2.1. Optical Polarization

The polarimetric observations have been done with the 0.60-m Boller & Chivens telescope at Observatório do Pico dos Dias, Brazil, operated by the Laboratório Nacional de Astrofísica (LNA),

Brazil, using a CCD camera modified by the polarimetric module described in Magalhães et al. (1996). The CCD array used was a SITe back-illuminated, 1024×1024 pixels. The above telescope and instrumentation gives a field-of-view of $10'.5 \times 10'.5$. The polarization in the V band was measured on 1999 April 11 and July 29; the observations in the $(RI)_C$ bands were also obtained on 1999 July 29 and in the B band, on 1999 July 30. In each night, we observed polarimetric standards stars (Serkowski, Mathewson, & Ford 1975; Bastien et al. 1988; Turnshek et al. 1990) in order to calibrate the system and estimate the instrumental polarization. The measured values of the unpolarized standard stars were consistent with zero within the errors: consequently no instrumental correction was applied. Measurements using a Glan filter were also performed to estimate the efficiency of the instrument. They indicate that no instrumental correction is needed.

The images have been reduced following the standard steps of differential photometry using the IRAF⁶ facility. Counts were used to calculate the polarization using the method described in Magalhães, Benedetti, & Roland (1984). The measured polarization of Hen 3-1475 is shown in Table 1. The aperture radius that minimizes photometry errors is 4 pixels (corresponding to $2.44''$ in the sky). It was kept constant for all bands. In the Discussion and Conclusion sections we will have in mind that the polarization measurements refer to an extended region in the vicinity of the central object in Hen 3-1475. The multicolor polarimetry was obtained in nights of poor photometric conditions with high sky counts. Although this does not have important consequences on polarization results, which are based on a differential technique, this precludes us from detecting the nebula surrounding the central object.

2.2. IR Photometry

Hen 3-1475 was observed with the CamIV NIR imager in the 1.6-m telescope of LNA on 1999 July 29. The detector is a HAWAII array, with $0.24''/\text{pixel}$ spatial resolution, covering $4' \times 4'$. J

⁶IRAF is distributed by National Optical Astronomy Observatories, which is operated by the Association of Universities for Research in Astronomy, Inc., under contract with the National Science Foundation.

($1.25\mu\text{m}$) and H ($1.65\mu\text{m}$) band images were obtained. This region is already available in the Two Micron All Sky Survey (2MASS) survey, which we used to calibrate our photometry. Our combined images have an effective exposure time of 210 s in J and 40 s in H and provide $S/N \approx 10$ for $H=17$. This is deeper than the 2MASS photometry at the same S/N , also with a better spatial resolution, allowing us to discuss the gross features of the reddening in the line-of-sight to Hen 3-1475. The J and H magnitudes for the target were obtained from short exposure time images and are $J = 9.75 \pm 0.01$ and $H = 8.44 \pm 0.01$.

3. Inter- and Circumstellar Reddening of Hen 3-1475

We have obtained the magnitudes of 213 objects around Hen 3-1475. An examination of the color-magnitude diagram (CMD) $H \times (J-H)$ allows us to put limits on the total reddening to this line of sight, since the distribution of unreddened stars is relatively localized. Hen 3-1475 has $l = 9.8^\circ, b = +5.3^\circ$, corresponding to a line-of-sight that intercepts a relatively dense part of the bulge of the Galaxy. The objects we observe with $H < 14$ and $(J-H) \approx +0.8$ probably are red giants in the bulge. If they were not subject to reddening, the distribution of their color indices should have a maximum around $J-H \approx +0.5$. This can be obtained by a simple implementation of the model of Wainscoat et al. (1992). Using the Cardelli, Clayton, & Mathis (1989) parametrization of the IS extinction curve, we obtain $E(J-H) = 0.09 A(V)$, for $R = 3.1$. So we conclude that the reddening to the red giants of the bulge is $A(V) \approx 3.2$ mag in this line-of-sight. If $R = 5$, $A(V)$ would change to 2.8 mag. These values are a bit larger than the previous estimate of Riera et al. (1995), $A(V) < 2.0 \pm 0.4$ mag.

The total reddening to Hen 3-1475 presents a much more complex problem, since the object is shrouded by circumstellar material. We assume an spectral type of B3 (Knapp et al. 1995). The object position in the CMD is not consistent with that of a dwarf, rather, a supergiant star is needed. Considering the color of a B3I (Tokunaga 2000), we can estimate a circumstellar $E(J-H)$ of 0.84 after subtracting the interstellar value. Converting the derived $E(J-H)$ to $A(V)$ is not straightforward.

A first guess could be made using a standard interstellar extinction law: this gives an intrinsic $A(V) = 9.1$ (7.9), if $R = 3.1$ (5.0). However, the spectral energy distribution of Hen 3-1475 may be quite different from that of a blue star attenuated by interstellar extinction law. At optical wavelengths the presence of scattered light - a blue component - may be important and at NIR wavelengths hot grains could have a non-negligible contribution to the spectrum. A model taking in account all these components will be explored in a forthcoming paper.

4. Discussion on polarimetric results

In this section, we present the estimates to the foreground and intrinsic polarization of Hen 3-1475. We also discuss a probable alignment between the intrinsic polarization of this object and the interstellar magnetic field. Finally, numerical modeling of Hen 3-1475 polarization is done assuming it is produced in a circumstellar disk.

4.1. Intrinsic polarization of Hen 3-1475

The observed polarization in astrophysical objects is usually the sum of two components: (i) the intrinsic one, produced in the object itself; (ii) the foreground component, which is produced in the interstellar medium (ISM) between the object and the Earth. The high polarization of Hen 3-1475 suggests that at least part of it may have an intrinsic origin because it is very unusual such a high value ($\approx 8\%$ in V band) to be produced in the ISM. To obtain the intrinsic component, it is necessary to estimate the foreground polarization and subtract it from the observed one.

The foreground polarization in each band was estimated by the weighted average polarization of all stars in the field-of-view. The results are presented in Table 1. As the line-of-sight to Hen 3-1475 is near the Galactic center ($l = 9.8^\circ; b = +5.3^\circ$), the images contain a large number of stars (see last column of Table 1). To illustrate the distribution of the polarization of the field stars we present histograms for their moduli and position angles in I_C band (Fig. 1.a and Fig. 1.b): notice that the maximum of each histogram coincides with the estimated values of the foreground polarization (Table 1). The histograms show single-mode distributions consistent with a sample of

stars coming from a singular population with regard to (interstellar) polarization properties. This may be interpreted as an evidence that the foreground dust shares the same properties all over this field. The histogram in Fig. 1.a also shows how large the polarization of Hen 3-1475 (arrow) is in comparison with the field stars. This reinforces the suspicion that this object has a large intrinsic component.

Another evidence to the intrinsic character of the Hen 3-1475 polarization comes from its wavelength dependence. We have fitted both the observed Hen 3-1475 polarization and that of the field stars with the Serkowski law (1973):

$$P(\lambda) = P_{max} \exp \left\{ -K \ln^2 \frac{\lambda_{max}}{\lambda} \right\}, \quad (1)$$

where: P_{max} is the maximum value of the polarization; λ_{max} is the wavelength where P_{max} occurs; and K is a parameter related to the curve width and dependent on λ_{max} (Serkowski, Mathewson & Ford 1975; Codina-Landaberry & Magalhães 1976; Wilking, Lebofsky, & Rieke 1982). In the fits, we have used $K = 1.66\lambda_{max} + 0.01$ (Whittet et al. 1992).

The results are shown in Table 2 and Figure 2: the polarization was normalized to P_{max} to allow an easier comparison between the curves. In this graph it is clear that the wavelength dependence of the polarization of Hen 3-1475 and the field stars are different. Also, λ_{max} occurs at a short wavelength for Hen 3-1475 when compared to the behavior of the field stars. Such a short value would be quite unusual if its origin was interstellar.

Based on the discussion above, we are confident that Hen 3-1475 has an intrinsic polarization produced in its circumstellar region. It was estimated subtracting the average polarization of the field stars from that observed for Hen 3-1475. These values are presented in Table 1. If we estimate the foreground polarization from a Serkowski law fit with a constant position angle, the changes in the intrinsic polarization are negligible. Hereafter, the term ‘‘Hen 3-1475 polarization’’ refers to its intrinsic value.

4.2. Geometry of Hen 3-1475 and its relation with the ISM

The Hen 3-1475 jets are aligned at approximately PA 135° (Riera et al. 1995; Bobrowski et al. 1995). The PA of the polarization, 42.1° (in V band), is consistent with the observed bipolar geometry: it is perpendicular to the jets and parallel to the dust torus. This behavior was already observed in young stellar objects with bipolar geometry (Hodapp 1984; Sato et al. 1985). The mechanism causing this polarization will be discussed in the Section 4.3: in this section we would like to discuss a possible correlation of the geometry of Hen 3-1475 with the orientation of the magnetic field of the surrounding ISM.

Curiously, the intrinsic polarization of Hen 3-1475 is nearly parallel to the polarization of the field stars (48.3° in V band). The latter effect is usually attributed to the transport of starlight through a dichroic medium. This dichroism is caused by non-spherical grains aligned by the interstellar magnetic field. Considering the standard model for grain alignment in the ISM, the polarization angle is parallel to the component of the magnetic field in the plane of the sky (Davis & Greenstein 1951; but see also Lazarian 2000). The foreground polarization direction in the field of Hen 3-1475 is almost parallel to the Galactic plane, which is at PA 33° . This result is consistent with those from maps of optical polarization that indicate that the direction of the magnetic field in the Galaxy follows the Galactic plane (Mathewson & Ford 1970; Axon & Ellis 1976).

The alignment between Hen 3-1475 geometry and field stars polarization can be interpreted as: (i) a chance effect; (ii) the foreground polarization is caused by a cloud physically near Hen 3-1475 and in this case the IS magnetic field aligning the grains is also present in the Hen 3-1475 environment; (iii) the cloud producing the polarization of field stars is far from Hen 3-1475 but its magnetic field is aligned with the Galactic plane, so the alignment of Hen 3-1475 may be regarded as relative to the Galactic plane.

Considering objects of similar evolutionary status, it is not clear if there is a correlation between the nebula axis and the Galactic plane. Recent results indicate that the symmetry axis of PNe are randomly distributed (Corradi, Aznar,

& Mampaso 1998). However, this work excluded PNe with small scale structures as the point symmetrical knots seen in Hen 3-1475, for instance. On the other hand, previous works had suggested some correlation between PNe axis and the Galactic plane (Melnick & Harwit 1975; Phillips 1997). Nebulae ejected by massive stars and bilateral supernova remnants seem to have their axis of symmetry along the Galactic plane (Hutsemekers 1999; Gaensler 1998). Possible mechanisms that could cause such a correlation are discussed in Melnick & Harwit (1975) and Phillips (1997).

Another possibility is that the axis of symmetry of Hen 3-1475 is determined by the IS magnetic field. The dust disk of Hen 3-1475 is probably a remnant of the AGB wind. It is quite unlikely that the IS magnetic field could have an important role in causing the asymmetry of the dense AGB wind⁷. Alternatively, the connection between an AGB stellar wind asymmetry and ISM might be a fossil from the star formation phase. Massive stars can indeed easily retain the main-sequence angular momentum (Garcia-Segura et al. 2001). We briefly present some results in the literature concerning the alignment of young stellar objects geometry with the IS magnetic field. This is still a mostly open subject in which studies using different techniques provide discordant results. Dyck & Lonsdale (1979) are among the first authors to notice a possible alignment between the direction of the IR polarization of protostellar sources and the IS magnetic field. Heckert & Zeilik (1981) show that IR polarization of YSOs tends to be parallel or perpendicular to the IS magnetic field. The large scale molecular outflow tends to be aligned with the IS magnetic field (Snell, Loren, & Plambeck 1980; Hodapp 1984; Cohen, Rowland & Blair, 1984; Vrba et al. 1986). Recent sub- and millimetric polarimetric studies of prestellar objects are not yet conclusive whether there is (or not) a correlation between the core elongation/outflow and the magnetic field of the containing filament (Ward-Thompson et al. 2000; Matthews & Wilson 2000; Glen, Walker, & Young 1999).

⁷Dgani (1998) has done some calculations showing that filamentary structures seen in old (=low density) PN can be explained on basis of their interaction with the magnetic field of the ISM.

4.3. Modeling the circumstellar environment of Hen 3-1475

To model the spectral dependence of the polarization in Hen 3-1475, we have used a three dimensional Monte Carlo code for radiative transfer in stellar envelopes (Rodrigues 1997; Rodrigues & Magalhães 2000). It includes scattering and absorption by dust particles, but their emission is neglected: therefore all the photons are originated in the central source. As we are modeling optical emission this can be considered as a reasonable approximation. The grains are considered spherical and homogeneous. We have used three optical constants in the models: astronomical silicate (Draine & Lee 1984 - DL94); O-rich silicate from Ossenkopf, Henning, & Mathis (1992 - O92); and amorphous carbon from Zubko et al. (1996 - Z96). The phase function considered is not the Henyey-Greenstein approximation, but the analytical function obtained from the Mie theory. The density, $\rho(r)$, was assumed to depend on the distance as r^{-2} .

The diameter of the Hen 3-1475 disk torus is about $2''$ (Borkowski et al. 1997). It was suggested that the jets are collimated near the first pair of knots, which is located around $3''$ from the central object (Borkowski et al. 1997). Therefore the aperture radius used in the polarization measurements includes the disk, but not the jets. So, the intrinsic polarization, as obtained in this work, should originate mainly by processing of the central source light in the optically thick disk torus. This configuration can indeed produce a polarization parallel to the disk as observed in objects with bipolar geometry (Bastien & Menard 1988; Hodapp 1984; Sato et al. 1985). This can be explained by multiple scattering in an optically thick disk (Bastien & Menard 1988, 1990; Whitney & Hartmann 1993; Fischer, Henning, & Yorke 1994). We have adopted a cylindrical geometry to represent the Hen 3-1475 disk.

The models have a relatively large number of input parameters (Table 3). In order to minimize the number of degrees of freedom, we have fixed a given parameter if it has a reasonable good published estimate - see in Table 3 whether a parameter was considered fixed, its value and the reference to the estimate. If Hen 3-1475 is at 8 kpc (Borkowski & Harrington 2001), $1''$ corresponds

to a physical size of 0.04 pc ($1.7 \times 10^6 R_{\odot}$). This value was used for the external radius of the disk. Its inner radius was estimated to be about 0.01 pc = $4 \times 10^5 R_{\odot}$ according to the IRAS fluxes (Borbrowski et al. 1995). This is consistent with simulations of formation of PN envelopes (Mellema & Frank 1995). To estimate the stellar radius we have considered a spectral type B3 (Knapp et al. 1995) and a luminosity of $25\,000 L_{\odot}$ (Borkowski & Harrington 2001), which results in a value of $20 R_{\odot}$. In a cylindrical geometry, there is one more parameter: the disk height, h , which we varied. We may notice that the results are invariant if all lengths are multiplied by a given factor and if the optical depth, τ , is kept constant. We can also fix the disk inclination, adopting the inclination angle of the bipolar outflow obtained from Borkowski & Harrington (2001), which is 40° .

Before analyzing the quantitative results for Hen 3-1475, we discuss how each parameter affects the polarization curve. In the optically thick regime, the optical depth controls basically the polarization degree and slightly the shape of the spectral polarization curve. The polarization curve obtained by a model with a distribution of grain sizes has a maximum at a wavelength related to the average grain size. The width of that curve is related to the width of the grain size distribution. In Hen 3-1475 we do not see the polarization maximum, but it may occur at smaller wavelengths than those covered by our observations. The cylinder height, h , plays a role that is not so obvious. For the present case, when we consider a fixed line of sight (= inclination), the height defines whether the central source light is blocked or not by the envelope: the more direct starlight, the smaller the polarization degree. Also, a thicker cylinder contains more matter, which also contributes to increase the polarization. Hence, the cylinder height strongly affects the polarization degree. Concerning the Hen 3-1475 polarization model, a small height allows the central object to be seen directly, producing a polarization that is not high enough. We conclude that the minimum cylinder height that is needed to fit the polarization is $h_{min} \approx 7. \times 10^5 R_{\odot}$.

We have initially tried to fit the wavelength dependence of the Hen 3-1475 polarization using a single grain size but the width of the obtained curves were too narrow, so a size distribution had

to be introduced. We have used the recipe of Mathis, Rumpl, & Nordsieck (1977 - MRN), the standard model for the interstellar medium grains. It is represented by a power-law, a^q , with adjustable limits, a_{min} and a_{max} .

In order to fit the Hen 3-1475 polarization data, we have proceeded in the following way: we fixed the parameters related to the envelope geometry and the index of the grain-size power-law distribution, q . Then, we let the the grain size distribution limits and the optical depth vary in order to find the best model in a weighted chi-square sense. The best fits are shown in Table 4.

Let's initially suppose a grain size distribution that has an exponent, q , of -3.5. In spite of having an oxygen-rich envelope (Knapp et al. 2000), the optical properties of amorphous carbon provide a better fit to Hen 3-1475 polarization data than the silicate ones. This is illustrated in Table 4 (see models 1, 5 and 7) and also in Fig. 3. This graph also shows that all models tend to produce polarization curves narrower than the observed. An improvement could be in principle obtained using less steep power-law grain size distributions. Varying the q index for an amorphous carbon model (see models 1, 2 and 3 and also Fig. 4), we could improve the chi-square (best fit for $q = -3.0$), but the shape of the polarization spectral curve was not well described yet. An improvement could also be achieved by decreasing the cylinder height (see model 4 and Fig. 5). The grain sizes of the models in Table 4 do not differ significantly, in spite of being obtained using models with different values of q and h : so the dust sizes are relatively well-constrained. Considering the best fit (model 4), the polarization of Hen 3-1475 can be fitted by amorphous carbon grains with size in the range 0.063 - 0.22 μm following a -3.0 power-law. We notice, however, that silicate is not discarded as a possible dust composition. A more refined model should be used to better constrain the chemical composition (see below). Table 4 shows that the grain sizes are moderately affected by the optical constants.

As mentioned above the measured polarization of Hen 3-1475 is parallel to the dust torus (see Table 1). Fig. 6 shows the degree and the position angle of the polarization obtained with the model 4. In the position angle panel a value of 90° corresponds to a polarization parallel to the disk:

this means that the BVRI observations are reproduced. However, the optical depth decreases to the red and in some point the envelope becomes optically thin, so the polarization could become perpendicular to the disk. This would produce a behavior similar to the Type 1c objects from Trammell et al. (1994): a rotation of 90° and a decreasing polarization from small (optically thick) to large wavelengths (optically thin). To check that possibility, we have calculated the JHK polarization produced by model 4, which is also shown in Fig. 6⁸. We see that the polarization decreases rapidly in the IR and remains parallel to the disk. Therefore the rotation is not observed in model 4. The same result is seen for amorphous carbon models of Carciofi, Magalhães, & Bjorkman (2002). The polarization modulus in NIR provided by the code must be seen with caution because the model does not include the dust (re)emission, which may be important at those wavelengths.

The absence of angle rotation in model 4 is caused by the large absorption of the amorphous carbon. If a less absorptive material was used (as silicate), the rotation could be produced. So the polarization angle restricts the envelope optical depth and also the index of refraction of the dust. This means that JHK polarization measurements would be useful to better determine the grain composition in the envelope of Hen 3-1475.

A more complete study of the dust torus of Hen 3-1475 using a code that includes the radiative transfer and the thermal equilibrium is being carried on (C. V. Rodrigues & A. C. Carciofi, in preparation). The flux from optical to IR wavelengths, as well as the polarization, will be modeled. This will put more constraints on the physical properties of the dust envelope of Hen 3-1475.

5. Conclusions

In this work we analyze BVRI polarization and IR photometry of the proto-planetary nebula Hen 3-1475. The main results are summarized below:

- the optical broad band fluxes of Hen 3-1475 are highly polarized. A large fraction of this

⁸The position angle in the K band obtained using a Monte Carlo code has a very large statistical error (see error bars) because the polarization modulus is small.

polarization may be produced in the circumstellar environment of this object;

- the BVRI polarization position angle is perpendicular to the axis of the bipolar structure seen in optical images. As the aperture used to measure the polarization is small and therefore does not include the jets, that implies that the central disk must be optically thick in all the bands observed or the dust must be composed of a highly absorptive material;
- the wavelength dependence of the polarization of Hen 3-1475 was modeled using a Monte Carlo radiative transfer code. We could find a good fit using an index -3.0 for the power-law grain-size distribution, whose limits are 0.063 and 0.22 μm . In spite of the claim for an oxygen chemistry envelope (Knapp et al. 2000), the optical constants of amorphous carbon produce a better fit to the optical polarization than those of silicates. However, the simple model used here does not allow to discard silicate dust in the Hen 3-1475 circumstellar envelope;
- our CCD images provide us with polarimetric data of a large number of stars in the Hen 3-1475 field. So we could reliably estimate the foreground polarization in this direction. Curiously, the foreground polarization has the same direction of the intrinsic polarization of Hen 3-1475. This might be interpreted as an interplay between the IS magnetic field and the Hen 3-1475 geometry;
- the IR colors of Hen 3-1475 suggests an interstellar reddening in the V band of around 3.2 mag in the line of sight. The circumstellar extinction was estimated as $A(V) \approx 9.0$ mag.

We are grateful to A. Damini for lending us observational time and to Alex C. Carciofi for suggestions to the manuscript. We also acknowledge the referee for the suggested improvements. JGH thanks FAPESP Proc. No. 2001/09018-2.

This publication makes use of data products from the Two Micron All Sky Survey, which is a

joint project of the University of Massachusetts and the Infrared Processing and Analysis Center/California Institute of Technology, funded by the National Aeronautics and Space Administration and the National Science Foundation.

This research has also made use of NASA's Astrophysics Data System Bibliographic Services and of the SIMBAD database, operated at CDS, Strasbourg, France.

REFERENCES

- Axon, D. J. & Ellis, R. S. 1976, MNRAS, 177, 499
- Bastien, P. & Menard, F. 1988, ApJ, 326, 334
- Bastien, P. & Menard, F. 1990, ApJ, 364, 232
- Bastien, P., Drissen, L., Menard, F., Moffat, A. F. J., Robert, C., & St-Louis, N. 1988, AJ, 95, 900
- Borkowski, K. J., Blondin, J. M., & Harrington, J. P. 1997, ApJ, 482, L97
- Borkowski, K. J. & Harrington, J. P. 2001, ApJ, 550, 778
- Bobrowski, M., Zijlstra, A. A., Grebel, E. K., Tinney, C. G., te Lintel Hekkert, P., van de Steene, G. C., Likkell, L., & Bedding, T. R. 1995, ApJ, 446, L89
- Carciofi, A. C., Bjorkman, J., & Magalhães, A. M. 2002, ApJ, submitted
- Carciofi, A. C., Magalhães, A. M., & Bjorkman, J. 2002, preprint
- Cardelli, J.A., Clayton, G.C., & Mathis, J.S. 1989, ApJ, 345, 245
- Codina-Landaberry, S. & Magalhães, A. M. 1976, A&A, 49, 407
- Cohen, R. J., Rowland, P. R., & Blair, M. M. 1984, MNRAS, 210, 425
- Corradi, R. L. M., Aznar, R., & Mampaso, A. 1998, MNRAS, 297, 617
- Davis, L. & Greenstein, J. L. 1951, ApJ, 114, 206
- Dgani, R. 1998, RMxAC, 7, 149
- Draine, B. T. & Lee, H. M. 1984, ApJ, 285, 89 (DL84)
- Dyck, H. M. & Lonsdale, C. J. 1979, AJ, 84, 1339
- Fischer, O., Henning, Th., & Yorke, H. W. 1994, A&A, 284, 187
- Frank, A. 2000, in Asymmetrical Planetary Nebulae II: From Origins to microstructures, ed. J. H. Kastner et al. (San Francisco: ASP), 225
- Frank, A., Lery, T., & Blackman, E. 2002, preprint (astro-ph/0207447)
- Gaensler, B. M. 1998, ApJ, 493, 781
- García-Segura, G., Franco, J., López, J. A., Langer, N., & Rózycka, M. 2002, RMxAC, 12, 117
- Gledhill, T. M., Chrysostomou, A., Hough, J. H., & Yates, J. A. 2001, MNRAS, 322, 321
- Glenn, J., Walker, C. K., & Young, E. T. 1999, ApJ, 511, 812
- Heckert, P. A. & Zeilik, M., II 1981, AJ, 86, 1076
- Heckert, P. A. & Smith, P. S. 1988, AJ, 95, 873
- Hodapp, K.-W. 1984, A&A, 141, 255
- Hutsemékers, D. 1999, A&A, 344, 143
- Johnson, J. J. & Jones, T. J. 1991, AJ, 101, 1735
- Kahn, F. D. & West, K. A. 1985, MNRAS, 212, 837
- Knapp, G. R., Bowers, P. F., Young, K., & Phillips, T. G. 1995, ApJ, 455, 293
- Knapp, G. R., Crosas, M., Young, K., & Ivezić, Z. 2000, ApJ, 534, 324
- Lazarian, A. 2000, in Cosmic Evolution and Galaxy Formation, ed. J. Franco et al. (San Francisco: ASP), 69
- Li, A. & Lunine, J. I. 2002, preprint (astro-ph/0207642)
- te Lintel Hekkert, P. 1991, A&A, 248, 209
- Magalhães, A. M., Benedetti, E., & Roland, E. H., 1984, PASP, 96, 383
- Magalhães A. M., Rodrigues C. V., Margoniner V. E., Pereyra A., & Heathcote S., 1996, in Polarimetry of the Interstellar Medium, ed. W. G. Roberge & D. C. B. Whittet (San Francisco: Astronomical Society of Pacific), 118
- Matthews, B. C. & Wilson, C. D. 2000, ApJ, 531, 868
- Mathewson, D. S. & Ford, V. L. 1970, MNRAS, 74, 139

- Mathis, J. S., Rimpl, W., & Nordsieck, K. H. 1977, *ApJ*, 217, 425
- Meixner, M., Ueta, T., Bobrowsky, M., & Speck, A. 2002, *ApJ*, 571, 936
- Mellema, G. & Frank, A. 1995, *MNRAS*, 273, 401
- Melnick, G. & Harwit, N. 1975, *MNRAS*, 171, 441
- Ossenkopf, V., Henning, Th., & Mathis, J. S. 1992, *A&A*, 261, 567 (O92)
- Phillips, J. P. 1997, *A&A*, 325, 755
- Riera, A., Garcia-Laro, P., Machado, A., Potasch, S. R., & Raga, A. C. 1995, *A&A*, 302, 137
- Rodrigues, C. V. 1997, Radiative transfer in hot star envelopes using the Monte Carlo method, PhD Thesis, Univ. de São Paulo
- Rodrigues, C. V. & Magalhães, A. M. 2000, *ApJ*, 540, 412
- Sánchez Contreras, C. & Sahai, R. 2001, *ApJ*, 553, L173
- Sato, S., Nagata, T., Nakajima, T. Nishida, M., Tanaka, M., & Yamashita, T. 1985, *ApJ*, 291, 708
- Scarrot, S. M. & Scarrot, R. M. J. 1995, *MNRAS*, 277, 277
- Serkowski, K. 1973, in *IAU 52 Symp., Interstellar Dust and Related Topics*, ed. J. M. Greenberg & H. C. van der Hulst (Dordrech-Reidel), 145
- Serkowski, K., Mathewson, D. S., & Ford, V. L. 1975, *ApJ*, 196, 261
- Snell, R. L., Loren, R. B., & Plambeck, R. L. 1980, *ApJ*, 239, L17
- Stasińska, G. & Szczerba, R. 1999, *A&A*, 352, 297
- Stasińska, G. & Szczerba, R. 2001, *A&A*, 379, 1024
- Tokunaga, A. T. 2000, in *Allen's Astrophysical quantities*, ed. A. N. Cox (New York: Springer-Verlag), 143
- Trammell, S. R., Dinerstein, H. L., & Goodrich, R. W. 1994, *AJ*, 108, 984
- Turnshek, D. A., Bohlin, R. C., Williamson, R. L., II, Lupie, O. L., Koornneef, J., & Morgan, D. H. 1990, *AJ*, 99, 1243
- Vrba, F. J., Luginbuhl, C. B., Strom, S. E., Strom, K. M., & Heyer, M. H. 1986, *AJ*, 92, 633
- Wainscoat, R.J., Cohen, M., Volk, K., Walker, H.J., & Schwartz, D.E. 1992, *ApJS*, 83, 111
- Ward-Thompson, D., Kirk, J. M., Crutcher, R. M., Greaves, J. S., Holland, W. S., & André, P. 2000, *ApJ*, 537, L135
- Whitney, B. A. & Hartmann, L. 1993, *ApJ*, 402,605
- Whittet, D. C. B., Martin, P. G., Hough, J. H., Rouse, M. F. Bailey, J. A., & Axon, D. J. 1992, *ApJ*, 386, 562
- Wilking, B. A., Lebofsky, M. J., & Rieke, G. H. 1982, *AJ*, 87, 695
- Zijlstra, Albert A., Chapman, J. M., te Lintel Hekkert, P., Likkell, L., Comeron, F., Norris, R. P., Molster, F. J., & Cohen, R. J. 2001, *MNRAS*, 322, 280
- Zubko, V. G., Mennella, V., Colangeli, L., & Bussoletti, E. 1996, *MNRAS*, 282, 1321 (Z96)

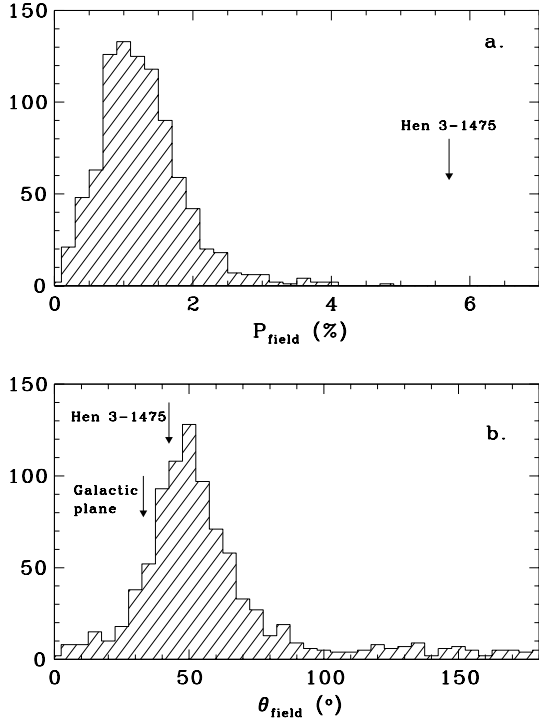


Fig. 1.— Histograms of the field stars polarization in I_c band: a. Polarization degree; b. Position angle.

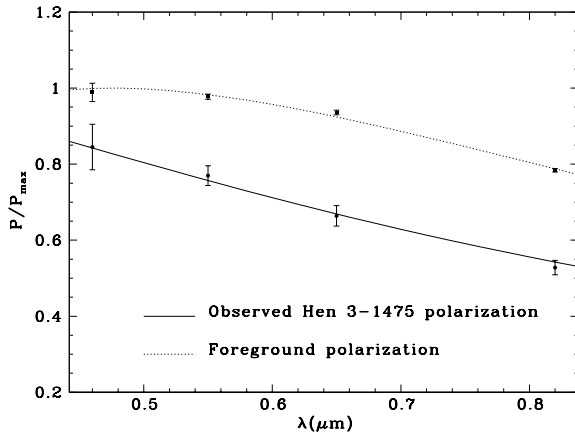


Fig. 2.— Polarization data and Serkowski fits to the polarization of Hen 3-1475 and field stars.

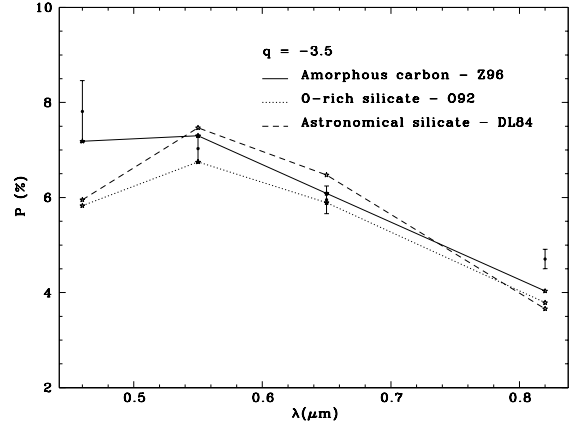


Fig. 3.— Models to the intrinsic polarization of Hen 3-1475 using different grain composition.

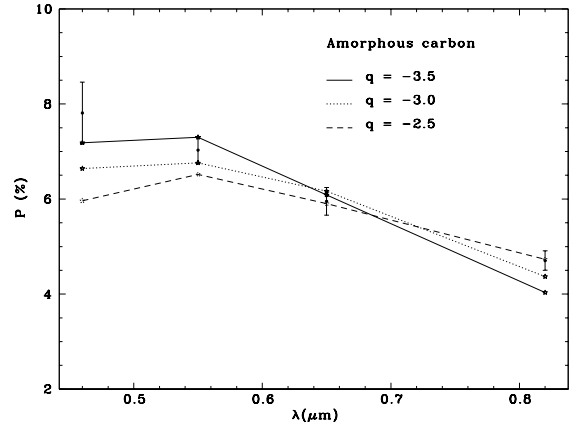


Fig. 4.— Models to the intrinsic polarization of Hen 3-1475 varying the index of the power-law size distribution.

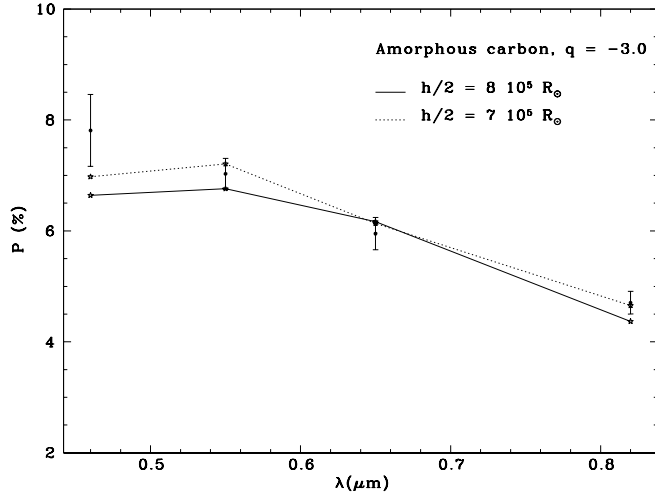


Fig. 5.— Models to the intrinsic polarization of Hen 3-1475 for different cylinder heights.

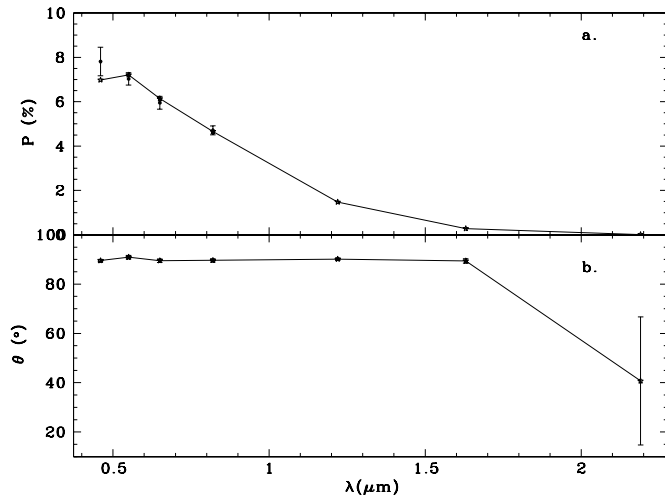


Fig. 6.— Polarization (a) and position angle (b) in the BVRIJHK bands for the best fit. The error bars in panel b are estimates to statistical error of the model.

TABLE 1
POLARIZATION OF HEN 3-1475 AND OF FIELD STARS

Object	Band	P (%)	σ (%)	θ ($^{\circ}$)	σ ($^{\circ}$)	Number of observations
Hen 3-1475 (Observed)	B	9.12	0.65	43.7	2.0	1
	V	8.31	0.28	43.1	1.0	2 ^a
	R _C	7.17	0.29	41.3	1.2	1
	I _C	5.70	0.20	40.2	1.0	1
Hen 3-1475 (Intrinsic)	B	7.81	0.65	43.7	2.4	-
	V	7.03	0.28	42.1	1.1	-
	R _C	5.95	0.29	40.2	1.4	-
	I _C	4.71	0.20	38.4	1.2	-
Field Stars	B	1.313	0.032	43.45	0.7	95
	V	1.298	0.009	48.30	0.2	501
	R _C	1.243	0.008	46.25	0.2	617
	I _C	1.041	0.006	47.99	0.2	901

^aaverage of the two observations

TABLE 2

SERKOWSKI LAW FITS TO THE OBSERVED POLARIZATION OF HEN 3-1475 AND TO THE FIELD STARS ($K = 1.66 \lambda_{max} + 0.01$ - WHITTET ET AL. 1992)

Object	P_{max} (%)	σ (%)	λ_{max} (μm)	σ (μm)	K	σ	χ^2
Hen 3-1475	10.8	3.3	0.24	0.18	0.40	0.30	0.74
Field stars	1.328	0.012	0.4746	0.0092	0.798	0.015	5.4

TABLE 3
INPUT PARAMETERS FOR THE POLARIZATION MODEL OF HEN 3-1475

Input parameter	Fixed	Value
Source radius	Yes	$20 R_{\odot}$ ^a
Internal radius of the disk, R_i	Yes	$4 \times 10^5 R_{\odot}$ ^b
External radius of the disk	Yes	$1.7 \times 10^6 R_{\odot}$ ^c
Height of the disk, h	No	$4 - 9 \times 10^5 R_{\odot}$
Inclination angle between disk axis and plane of sky	Yes	40° ^d
Optical depth in V band, τ_V	No	Fitted
Minimum limit of the size distribution, a_{min}	No	Fitted
Maximum limit of the size distribution, a_{max}	No	Fitted
Exponent of the size distribution, q	No	-3.5 to -2.5
Refractive index	Yes	Literature ^e

^aEstimated in this work

^bFrom the IRAS fluxes (Bobrowski et al. 1995)

^cFrom optical image (Riera et al. 1995; Bobrowski et al. 1995)

^dFrom optical spectroscopy (Borkowski & Harrington 2001)

^eSee text

TABLE 4

PARAMETERS OF THE MODELS FOR THE SPECTRAL DEPENDENCE OF THE POLARIZATION OF HEN 3-1475

Model	Material	q	$h/2$ (R_{\odot})	τ_V	a_{min} (μm)	a_{max} (μm)	χ^2
1	Amorphous carbon - Z96	-3.5	8×10^5	9.0	0.063	0.21	13.0
2	Amorphous carbon - Z96	-3.0	8×10^5	9.0	0.064	0.21	7.5
3	Amorphous carbon - Z96	-2.5	8×10^5	9.0	0.062	0.21	11.6
4	Amorphous carbon - Z96	-3.0	7×10^5	12.5	0.063	0.22	2.5
5	Silicate O-rich - O92	-3.5	8×10^5	9.0	0.072	0.26	30.7
6	Silicate O-rich - O92	-3.0	8×10^5	9.5	0.070	0.26	19.2
7	Astronomical silicate - DL84	-3.5	8×10^5	9.0	0.064	0.29	39.9